Rotationally resolved spectrum of the $C\ ^2\Pi_u \leftarrow X\ ^2\Pi_g$ electronic transition of C_4^- via resonant two-photon detachment spectroscopy

Yuexing Zhao, Esther de Beer,[a] and Daniel M. Neumark[b]
Department of Chemistry, University of California, Berkeley, California 94720 and Chemical Sciences Division, Lawrence Berkeley National Laboratory, Berkeley, California 92470

(Received 26 February 1996; accepted 6 May 1996)

The $C\ ^2\Pi_u \leftarrow X\ ^2\Pi_g$ electronic transition of C_4^- has been studied by both one-color and two-color resonant two-photon detachment (R2PD) spectroscopy. The one-color spectrum reveals vibrational structure in the excited anion state. Transitions due to excitations in one of the symmetric stretching modes as well as the bending modes are observed. Spectral resolution in the one-color experiment is limited by power broadening; using two-color R2PD, rotationally resolved spectra of the origin and 2_0^1 bands of the $C\ ^2\Pi_u \leftarrow X\ ^2\Pi_g$ transition are obtained. Molecular constants determined by fitting the rotationally resolved spectra are generally in good agreement with a recent *ab initio* calculation by Schmatz and Botschwina [Int. J. Mass. Spec. Ion. Proc. **149**, 621 (1995)]. Perturbations in the 2_0^1 band are attributed to Fermi resonance interactions in the $C\ ^2\Pi_u$ state. [S0021-9606(96)00631-9]

I. INTRODUCTION

The properties of carbon clusters have been of intense interest to chemists for many years.[1] It is only recently, however, that the techniques of high resolution spectroscopy have been successfully applied to these species. In 1989, according to the classic review article by Weltner and van Zee,[2] rotationally resolved spectra had only been measured for C_2 and C_3. Since then, rotationally resolved spectra have been obtained for several larger linear carbon clusters, primarily through infrared absorption spectroscopy;[3] among other things, these spectra show that carbon clusters as large as C_{13} exist as stable linear isomers.[4] It has been considerably more difficult to obtain high resolution spectra of carbon cluster ions. Prior to the work reported here, C_2^- was the only such species for which rotationally resolved spectra had been measured.[5–9] In this paper, we present the rotationally resolved electronic spectrum of C_4^- obtained with resonant two-photon detachment (R2PD).

C_4^- has been generated in the gas phase by a number of methods,[10] but only a few experiments have yielded information on its spectroscopy and structure. Photoelectron spectroscopy[11,12] of C_4^- indicates that C_4^- is a linear anion, and that linear C_4 has an electron affinity (EA) of 3.882 $\pm$0.010 eV. The linear structure for the anion inferred from the photoelectron spectra is supported by ion chromatography experiments.[13] In a recent mass-selected matrix absorption study, Maier[14] located an electronic transition in C_4^- with T_0=2.71 eV, and assigned it to a $^2\Pi \leftarrow X\ ^2\Pi$ transition.

On the theoretical side, *ab initio* calculations of the electron affinities of C_4 as well as the geometries of the linear anion and neutral ground states have been carried out by Bartlett[15] and Adamowicz.[16,17] The electronic spectroscopy of C_4^- has also been investigated. Adamowicz[17] calculated the vertical excitation energies of several low-lying excited states of C_4^-, finding three low-lying excited doublet states: the $A\ ^2\Sigma_g^+$, $B\ ^2\Sigma_u^+$, and $C\ ^2\Pi_u$ states. Recently, Schmatz and Botschwina[18] performed large-scale open-shell coupled cluster calculations on C_4^-, and obtained spectroscopic constants for the ground $X\ ^2\Pi_u$ state and the three excited doublet states. Based on these calculations, Botschwina assigned the C_4^- transition at 2.71 eV to the $C\ ^2\Pi_u \leftarrow X\ ^2\Pi_g$ transition.

The matrix value of T_0 for the $C\ ^2\Pi_u \leftarrow X\ ^2\Pi_g$ transition is greater than half of the EA. One can therefore access this transition in the gas phase using the very high sensitivity afforded by resonant two-photon detachment (R2PD), as was first demonstrated in the study of C_2^- by Lineberger.[19] In this paper, we report one- and two-color R2PD spectra of C_4^-. The lower-resolution (0.3 cm^{-1}) one-color spectrum from 21 600–24 900 cm^{-1} shows vibrationally resolved structure. Our spectrum is in qualitative agreement with Maier's matrix results.[14] However, additional features due to vibrational excitation in the bending modes are observed in our spectrum. Higher resolution (0.05 cm^{-1}) two-color experiments show rotationally resolved structure in selected regions of the spectrum. Molecular constants are determined for both electronic states by fitting the observed rotational line positions.

II. EXPERIMENT

The ion beam apparatus used in these experiments has been described in detail elsewhere.[20,21] Although the instrument was originally designed for negative ion zero electron kinetic energy (ZEKE) experiments, it can also measure photodetachment cross sections as a function of photon energy, and this is what is needed for the experiments described here.

Carbon cluster anions are generated in a pulsed discharge source which has been described previously.[22] Briefly, a gas mix of 3% acetylene, 1% CO_2 in Ne is pulsed from a piezoelectric valve and passes through the discharge

[a]Current address: Ultrafast Laser and Spectroscopy Laboratory, Department of Chemical Physics and Material Science Center, University of Groningen, Nijenborgh 4, 9747 AG Groningen, The Netherlands.
[b]Camille and Henry Dreyfus Teacher–Scholar.

region in which a pulsed electric field is applied just after the valve opens. The resulting mixture of ions and neutrals passes through a short clustering channel (5 mm long, 2.5 mm I.D.) prior to expansion into the source vacuum chamber. To improve stability of the ion signal, a 1 keV electron beam intersects the expanding molecular beam. The pulsed beam then passes through a 2 mm diam skimmer 1.5 cm from the discharge assembly and into the next vacuum region. We found that the distance between the pulsed valve and the skimmer strongly affects the temperature of the negative ions, with the temperature dropping as this distance is increased.

Negative ions that pass through the skimmer are collinearly accelerated to 1 keV. Ions are separated according to their mass-to-charge ratios in a 2 m coaxial beam-modulated time-of-flight mass spectrometer. The mass-selected ion packet is crossed by the laser beams, and all the electrons generated via photodetachment are extracted perpendicularly by a weak electric field and collected by a 40 mm diam multichannel plate (MCP) detector. The ion signal is monitored by another MCP detector that lies along the ion beam axis about 20 cm downstream from the laser interaction region. The electron signal is normalized to the ion signal and laser power.

In the one-color experiments, a single laser pulse is used to excite and photodetach the C_4^- anions via R2PD. A dye laser pumped by a XeCl excimer laser is used in these studies. The tuning element of this laser system is the grating of the dye laser. The measured bandwidth is ca. 0.3 cm^{-1}. The laser fluence used in this type of experiments is typically around 30 mJ/cm^2. To obtain the wavelength scans reported here, the following laser dyes are used: Coumarin 460, Coumarin 440, Exalite 416, and DPS.

The high photon fluence in the one-color experiments is required in order to achieve sufficient detachment. Unfortunately, this level of fluence saturates the bound–bound excitation transition and results in power broadening of the spectrum. This problem is solved by carrying out a two-color R2PD experiment. In the two-color experiment, the first laser pulse, which has weak photon fluence, excites the ion from its ground state to the excited electronic state. The second laser pulse, with smaller photon energy but much higher photon fluence, then detaches the electron from the excited anion. During the experiment, the frequency of the excitation laser pulse is tuned while that of the photodetachment pulse is fixed.

In the two-color experiments, the excitation laser pulse comes from the same excimer-pumped dye laser used in the one-color experiments. However, in order to obtain rotationally resolved spectra, a solid state intracavity etalon is used to obtain a narrower bandwidth of 0.04–0.07 cm^{-1}. The excitation laser fluence is kept around 1 mJ/cm^2 to reduce power broadening. No detectable C_4^- ions are detached with this amount of laser fluence. The second laser beam, either from a YAG-pumped dye laser or the second harmonic output of a YAG laser, is used to detach the photoexcited ions. The wavelength of the second laser beam is fixed at either 588 or 532 nm. Typical laser fluence of this laser beam is ca. 40 mJ/cm^2. This laser alone does not detach ground state C_4^-, because it is not resonant with an electronic transition. Photoelectrons generated by the second laser beam are collected as a function of the wavelength of the first laser beam. We find that electron signal intensity changed very little when the time delay between the two laser pulses is varied from 0 to 200 ns. This observation along with the multiphoton detachment mechanism will be discussed in detail in a related paper.[23] For the spectra reported here, the two laser pulses are separated by 120 ns temporally. The laser beams are also spatially separated by 6 mm along the axis of ion beam so that they interact with the same ions.

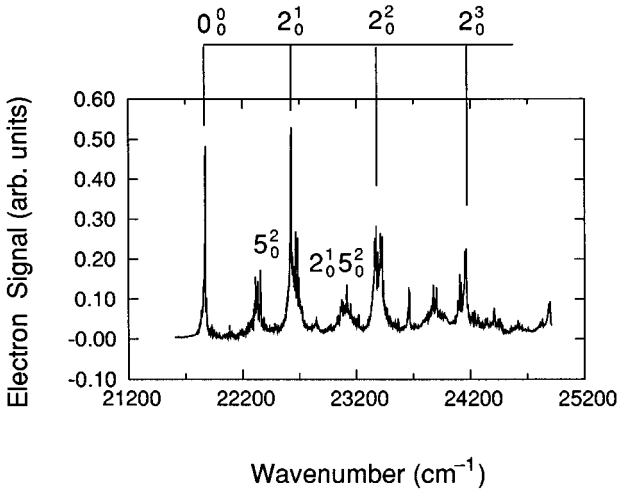

FIG. 1. One-color resonant two-photon detachment spectrum of C_4^-.

In the two-color scans, the intracavity etalon is stepped in intervals of 0.02 cm^{-1} every 80–100 laser shots. A total of 3–5 such scans are summed. Wavelength calibrations are performed immediately after the scans are taken. Absolute wavelength calibration is obtained by taking the absorption spectrum of a Fe–Neon discharge lamp. Relative calibration at wavelengths between the observed neon lines is obtained by recording the fringe spectrum of a solid state monitor etalon with a free spectral range of 0.67 cm^{-1}.

III. RESULTS

The one-color R2PD spectrum of C_4^- from 21 600 to 24 900 cm^{-1} is shown in Fig. 1. The peak positions, spacings and assignments (see below) are given in Table I. The spectrum appears to consist of a single electronic band, the origin of which is at 21 872 cm^{-1}. The most prominent feature of this band is a vibrational progression of four peaks with a spacing of ca. 750 cm^{-1}. In addition, there is a broad peak lying 450 cm^{-1} to the blue of each member of the main progression. Each peak consists of several partially resolved features.

Higher resolution two-color R2PD scans were taken at the origin and at the next strong transition at 22 630 cm^{-1}. The resulting spectra are shown in Fig. 2. Rotational structure is well resolved in these spectra, particularly for the

TABLE I. Peak positions, relative energies, assignments, and vibrational frequencies from one-color resonant two-photon detachment spectrum of the $C\ ^2\Pi_u \leftarrow X\ ^2\Pi_g$ transition in C_4^-.

Peak position (nm)	Peak position (cm^{-1})	Relative energies (cm^{-1})	Assignment	Frequencies (cm^{-1}) Expt.	Calc.
457.2	21 872	0	origin		
448.2	22 311	445	5_0^2	π_u 223	250[a]
441.9	22 630	750	2_1^0	σ_g 750	777[b]
433.4	23 073	1198	$2_0^1 5_0^2$		
428.0	23 364	1490	2_0^2		
422.6	23 663	1792			
418.8	23 878	2005			
414.8	24 108	2234	2_0^3		

[a]The calculated π_u frequency at UHF/6-31G* level using GAUSSIAN 92.
[b]From Ref. 18.

origin scan; typical peak widths are 0.1 cm^{-1}. There are two prominent band heads, labeled $R_{3/2}$ and $R_{1/2}$, toward the blue end of each spectrum. The separation between the two band heads is noticeably smaller in the origin scan than in the higher energy scan: 1.5 vs 6.4 cm^{-1}.

We also attempted to look at the transition near 22 320 cm^{-1} with two-color R2PD, but were unable to resolve individual rotational lines in this band.

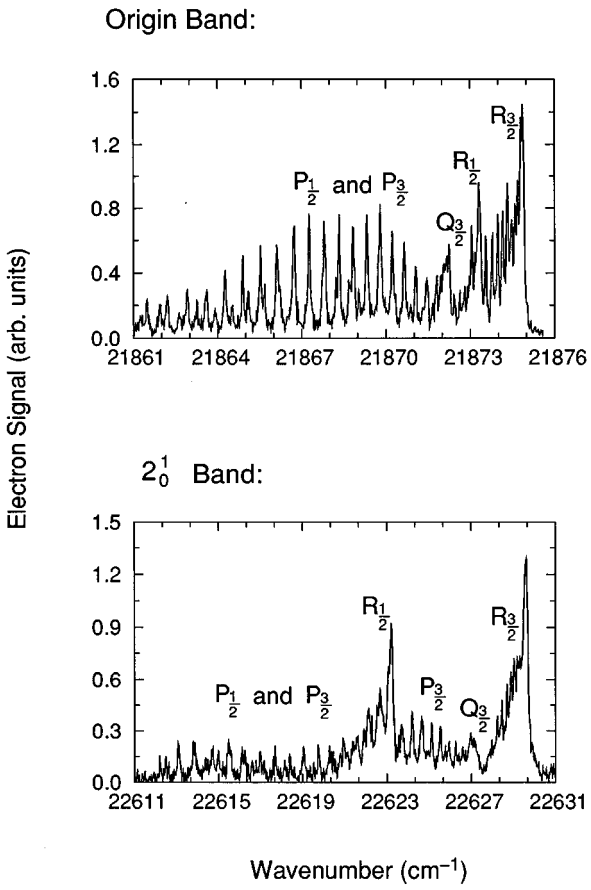

FIG. 2. High resolution two-color resonant multiphoton detachment spectrum of C_4^-.

IV. ANALYSIS AND DISCUSSION

A. One-color spectrum

The one-color spectrum in Fig. 1 clearly corresponds to the matrix absorption spectrum assigned by Maier[14] to C_4^-. The origin band in our spectrum occurs 24 cm^{-1} to the red of that in matrix spectrum, indicating a relatively small matrix shift, and a four-peak vibrational progression with a 750 cm^{-1} characteristic spacing is seen in both spectra. Schmatz and Botschwina[18] calculate the electronic term energy of the $C\ ^2\Pi_u$ state to be 22 600 cm^{-1} and one of its totally symmetric vibrational frequencies, the ν_2 symmetric stretch mode, to be 777 cm^{-1}. By comparison, we assign the structures in our spectrum to the $C\ ^2\Pi_u \leftarrow X\ ^2\Pi_g$ electronic transition of C_4^- and the main progression to the 2_0^n progression, in agreement with Maier's assignment. Franck–Condon activity in the ν_2 mode is consistent with the calculated geometries[18] which predict that the central C–C bond lengthens by 0.15 Å upon excitation of the $C\ ^2\Pi_u \leftarrow X\ ^2\Pi_g$ transition.

The peaks lying 446 cm^{-1} to the blue of the members of the 2_0^n progression were not seen in the matrix spectrum. These most likely involve double-quanta excitations in one of the low frequency bend modes of the $C\ ^2\Pi_u$ state. The bending frequency thus obtained, 223 cm^{-1}, is in good agreement with the *ab initio* $\nu_5(\pi_u)$ frequency of the $C\ ^2\Pi_u$ state, calculated by us at the UHF/6-31G* level to be 250 cm^{-1} (only frequencies for the totally symmetric modes were calculated in Ref. 18). We therefore assign these peaks to the $2_0^n 5_0^2$ progression.

The additional features seen in our spectrum but not in the matrix spectrum are most likely due to saturation effects in the one-color R2PD spectrum. The bound–bound excitation transition is considerably stronger than the bound-free photodetachment transition, so the high laser fluence needed to achieve sufficient photodetachment signal begins to saturate the excitation transition. This is evident from the power-broadening seen in the one-color experiments. Under such circumstances, strong vibrational transitions within the electronic band are more likely to saturate than the weaker ones, and the intensity of the weaker transitions would be greater

than would be predicted based on Franck–Condon factors alone. Transitions involving double excitation in nontotally symmetric modes are allowed by symmetry but are normally much weaker than transitions involving excitation in totally symmetric modes. The appearance of $2_0^n 5_0^2$ transitions in our spectrum but not in the matrix work is therefore most likely due to saturation of the bound–bound transition in our experiment.

B. Two-color spectrum

Before analyzing the high resolution data, a brief discussion of the $C\ ^2\Pi_u \leftarrow X\ ^2\Pi_g$ transition in C_4^- is in order. Although the spin–orbit coupling constant of C_4^- is not known, one would expect it to be close to that of C_5^- and C_6^-. The spin–orbit constants are known for the $X\ ^2\Pi_u$ states of C_5^- and C_6^- from ZEKE spectroscopy of these two negative ions and are found to be 26 and 29 cm^{-1}, respectively.[20,24] The rotational constant of C_4^- is calculated[18] to be around 0.16 cm^{-1}, which is much smaller than the spin–orbit splitting. Therefore, the rotational fine structure of C_4^- should belong to Hund's case (a). Because the molecular orbital configurations of the $X\ ^2\Pi_g$ and $C\ ^2\Pi_u$ states are $...1\pi_u^4 1\pi_g^3$ and $...1\pi_u^3 1\pi_g^4$, respectively, the $\Omega=3/2$ state of each electronic state should be lower-lying than the $\Omega=1/2$ state. In a $^2\Pi_u \leftarrow {}^2\Pi_g$ electronic transition, if both electronic states belong to Hund's case (a), each of the $^2\Pi_{3/2} \leftarrow {}^2\Pi_{3/2}$, $^2\Pi_{1/2} \leftarrow {}^2\Pi_{1/2}$ manifolds should have six branches (two P, two Q and two R). However, due to nuclear spin statistics, one Λ-doublet level is missing for each J level. As a consequence, one member of each pair of branches will be missing, resulting in only one P, one Q and one R branch for each spin–orbit manifold.

Figure 3 shows the first few rotational levels for the $^2\Pi_u$ and $^2\Pi_g$ states. The rotational levels are labeled by the total angular momentum J. The F_1 and F_2 manifolds correspond to the $^2\Pi_{3/2}$ and $^2\Pi_{1/2}$ spin–orbit states, respectively. The dashed lines represent the levels that are not populated due to nuclear spin statistics. The e/f parity labeling for each J level is determined using a scheme suggested by Kopp and Hougen,[25] and Brown *et al.*[26] The six transitions from the $J=7/2$ levels are shown; each of these transitions represents one transition in each of the six branches.

In the origin band of the rotationally resolved C_4^- spectrum, shown in the top half of Fig. 2, the six $P_{3/2}$, $Q_{3/2}$, $R_{3/2}$, $P_{1/2}$, $Q_{1/2}$, and $R_{1/2}$ branches, are all present. However, the $Q_{1/2}$ branch, i.e., the Q branch of the $^2\Pi_{1/2} \leftarrow {}^2\Pi_{1/2}$ manifold, is buried underneath the $P_{3/2}$ branch. The P and R branches are rotationally resolved; the $Q_{3/2}$ branch is partially resolved. In general the transitions in the $\Omega=1/2$ manifold are less intense because the cooling achieved in the free jet ion source favors the lower energy $^2\Pi_{3/2}$ state. Peaks in the P and R branches are assigned using combination differences. The peak positions and J level assignments are listed in Table II. The first transition in the $P_{3/2}$ branch is the $P(5/2)$ transition, which confirms our assignment of the $^2\Pi_{3/2}$ state as the ground state. The assignment of peaks in the partly resolved $Q_{3/2}$ branch is aided by the molecular parameters estimated from fitting the peaks in the P and R branches.

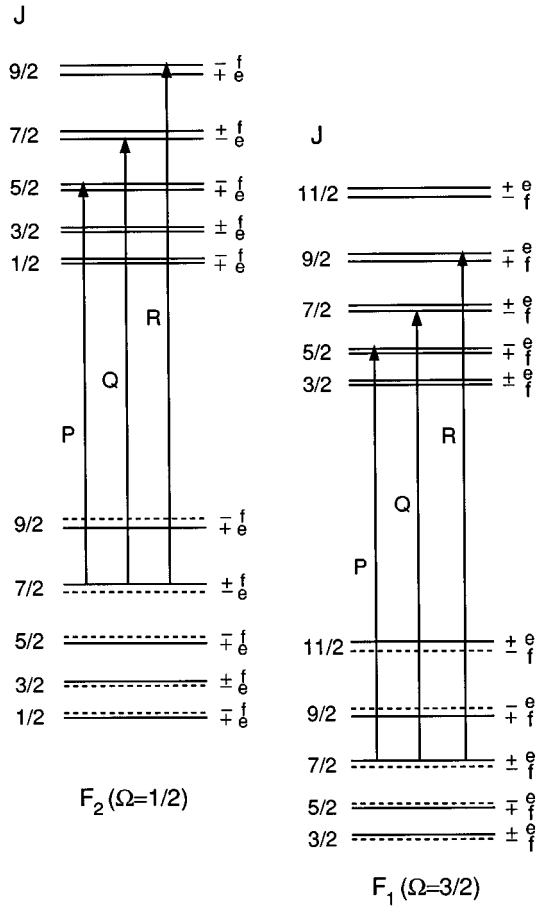

FIG. 3. Energy levels of the $X\ ^2\Pi_g$ and $C\ ^2\Pi_g$ states C_4^-. The six possible transitions originating from $J''=7/2$ are shown.

The same six branches are expected for the 2_0^1 band, but only the $P_{3/2}$ and $R_{3/2}$ branches could be assigned through combination differences; the $P_{1/2}$ branch is too weak to pick out individual transitions. The assigned peaks in this band are also listed in Table II.

Once the peak assignments have been completed, the line positions are fit to the effective rotational Hamiltonian derived by Zare *et al.*[27] using a nonlinear least-squares fitting program. The parameters used for each electronic and vibrational state were T_ν, the electronic and vibrational term energy (with T_0 of $X\ ^2\Pi_g$ state set to 0); B_ν and D_ν, the rotation and distortion constants, respectively; p_ν and q_ν, the Λ-doubling parameters as defined in Ref. 27; and A_ν, the spin–orbit coupling constant. (In the discussion below, $\nu=1$ refers to the $v_2=1$ vibrational level.) The appropriate Hund's case (a) matrix elements for a $^2\Pi$ molecule were taken from Neumark *et al.*[28] The above parameters were determined by a nonlinear least-squares fit based on the method of Marquardt that combines the Gauss method and the method of steepest descent.[29]

The origin band and the 2_0^1 band are fit separately. All the lines listed in Tables II and III are included in the fitting. Line positions were weighted according to their uncertain-

TABLE II. Observed transitions of the origin band of the $C\ ^2\Pi_u \leftarrow X\ ^2\Pi_g$ transition in C_4^- from the two-color resonant two-photon detachment spectrum (in cm^{-1}). Numbers in parentheses indicate estimated uncertainty of last digit.

	Observed	(Obs.−Calc.)×10^2
F_1 manifold (Ω=3/2)		
$P(2.5,f\rightarrow f)$	21 871.45(2)	1
$P(3.5,e\rightarrow e)$	21 871.06(2)	0
$P(4.5,f\rightarrow f)$	21 870.66(2)	0
$P(5.5,e\rightarrow e)$	21 870.23(2)	0
$P(6.5,f\rightarrow f)$	21 869.80(2)	1
$P(7.5,e\rightarrow e)$	21 869.32(2)	−1
$P(8.5,f\rightarrow f)$	21 868.83(3)	−1
$P(9.5,e\rightarrow e)$	21 868.34(2)	0
$P(10.5,f\rightarrow f)$	21 867.80(3)	−2
$P(11.5,e\rightarrow e)$	21 867.26(2)	−1
$P(12.5,f\rightarrow f)$	21 866.73(3)	2
$P(13.5,e\rightarrow e)$	21 866.12(2)	−1
$P(14.5,f\rightarrow f)$	21 865.53(2)	1
$P(15.5,e\rightarrow e)$	21 864.90(2)	0
$P(16.5,f\rightarrow f)$	21 864.26(2)	0
$P(17.5,e\rightarrow e)$	21 863.60(2)	1
$P(18.5,f\rightarrow f)$	21 862.91(2)	0
$P(19.5,e\rightarrow e)$	21 862.21(2)	0
$P(20.5,f\rightarrow f)$	21 861.49(2)	0
$P(21.5,e\rightarrow e)$	21 860.75(3)	1
$P(22.5,f\rightarrow f)$	21 859.98(2)	0
$P(23.5,e\rightarrow e)$	21 859.19(2)	−1
$P(24.5,f\rightarrow f)$	21 858.40(3)	0
$P(25.5,e\rightarrow e)$	21 857.61(5)	3
$P(26.5,f\rightarrow f)$	21 856.77(5)	1
$R(1.5,e\rightarrow e)$	21 873.05(3)	0
$R(2.5,f\rightarrow f)$	21 873.31(3)	−1
$R(3.5,e\rightarrow e)$	21 873.55(2)	−1
$R(4.5,f\rightarrow f)$	21 873.78(2)	0
$R(5.5,e\rightarrow e)$	21 873.98(2)	0
$R(6.5,f\rightarrow f)$	21 874.16(2)	0
$R(7.5,e\rightarrow e)$	21 874.32(2)	0
$R(8.5,f\rightarrow f)$	21 874.46(2)	0
$R(9.5,e\rightarrow e)$	21 874.59(2)	1
$R(10.5,f\rightarrow f)$	21 874.69(2)	0
$R(11.5,e\rightarrow e)$	21 874.78(3)	1
$Q(2.5,f\rightarrow e)$	21 872.24(3)	2
$Q(3.5,e\rightarrow f)$	21 872.16(2)	1
$Q(4.5,f\rightarrow e)$	21 872.06(2)	0
$Q(5.5,e\rightarrow f)$	21 871.97(3)	2
$Q(6.5,f\rightarrow e)$	21 871.81(2)	−1
F_2 manifold (Ω=1/2)		
$P(3.5,f\rightarrow f)$	21 869.48(2)	−1
$P(4.5,e\rightarrow e)$	21 869.06(5)	−3
$P(5.5,f\rightarrow f)$	21 868.68(3)	2
$P(6.5,e\rightarrow e)$	21 868.22(2)	1
$P(9.5,f\rightarrow f)$	21 866.79(6)	4
$P(10.5,e\rightarrow e)$	21 866.22(2)	0
$P(11.5,f\rightarrow f)$	21 865.67(2)	0
$P(12.5,e\rightarrow e)$	21 865.10(2)	0
$P(13.5,f\rightarrow f)$	21 864.52(2)	1
$P(14.5,e\rightarrow e)$	21 863.91(2)	0
$P(15.5,f\rightarrow f)$	21 863.27(2)	−1
$P(16.5,e\rightarrow e)$	21 862.63(2)	0
$P(17.5,f\rightarrow f)$	21 861.96(2)	0
$P(18.5,e\rightarrow e)$	21 861.27(2)	0
$P(19.5,f\rightarrow f)$	21 860.56(2)	0
$P(20.5,e\rightarrow e)$	21 859.84(3)	1
$P(21.5,f\rightarrow f)$	21 859.07(2)	−1
$R(5.5,f\rightarrow f)$	21 872.43(2)	−1
$R(6.5,e\rightarrow e)$	21 872.63(3)	1
$R(7.5,f\rightarrow f)$	21 872.80(3)	2
$R(8.5,e\rightarrow e)$	21 872.90(3)	−2

TABLE III. Observed transitions of the 2_0^1 band of the $C\ ^2\Pi_u \leftarrow X\ ^2\Pi_g$ transition of C_4^- from the two-color resonant two-photon detachment spectrum (in cm^{-1}). Numbers in parentheses indicate estimated uncertainty of last digit.

	Observed	(Obs.−Calc.)×10^2
F_1 manifold (Ω=3/2)		
$P(2.5,f\rightarrow f)$	22 626.30(6)	−3
$P(3.5,e\rightarrow e)$	22 625.94(4)	−1
$P(4.5,f\rightarrow f)$	22 625.54(2)	0
$P(5.5,e\rightarrow e)$	22 625.13(2)	1
$P(6.5,f\rightarrow f)$	22 624.66(3)	−1
$P(7.5,e\rightarrow e)$	22 624.19(4)	−2
$P(8.5,f\rightarrow f)$	22 623.70(3)	−2
$P(9.5,e\rightarrow e)$	22 623.19(3)	−2
$P(10.5,f\rightarrow f)$	22 622.67(2)	−1
$P(11.5,e\rightarrow e)$	22 622.14(2)	1
$P(12.5,f\rightarrow f)$	22 621.59(5)	3
$P(13.5,e\rightarrow e)$	22 620.98(4)	1
$P(14.5,f\rightarrow f)$	22 620.35(3)	0
$P(15.5,e\rightarrow e)$	22 619.72(2)	0
$P(16.5,f\rightarrow f)$	22 619.07(2)	1
$P(17.5,e\rightarrow e)$	22 618.38(2)	0
$P(18.5,f\rightarrow f)$	22 617.68(2)	0
$P(19.5,e\rightarrow e)$	22 616.97(2)	1
$P(20.5,f\rightarrow f)$	22 616.22(3)	0
$R(1.5,e\rightarrow e)$	22 627.97(5)	3
$R(2.5,f\rightarrow f)$	22 628.23(5)	3
$R(3.5,e\rightarrow e)$	22 628.46(4)	2
$R(4.5,f\rightarrow f)$	22 628.68(5)	2
$R(5.5,e\rightarrow e)$	22 628.88(5)	2
$R(6.5,f\rightarrow f)$	22 629.03(3)	−1
$R(7.5,e\rightarrow e)$	22 629.19(3)	0

ties, typically 0.02–0.03 cm^{-1}. The origin band is fit first. Some of the best-fit parameters are shown in Table IV. These parameters are obtained by simultaneously fitting all the molecular parameters. In fitting the 2_0^1 band, the ground state parameters are held fixed at the values obtained from the origin band. These two bands both originate from the ground electronic state, but many more lines are resolved in the origin band and the signal-to-noise ratio is also better in the origin band. The differences between the observed and calculated line positions are displayed in Tables II and III. Table IV also shows the results of the *ab initio* calculation by Schmatz and Botschwina.[18]

The rotational constants are in excellent agreement with the *ab initio* values.[18] Although the *ab initio* rotational constant B_e is calculated at the equilibrium geometry, the small value of α_2 for the $C\ ^2\Pi_g$ state indicates that $B_e \cong B_0$, so the comparison between B_0 and B_e is valid for the $C\ ^2\Pi_g$ state and probably for the ground state, too.

The fitting procedure yields uncertainties in the Λ-doubling parameters, p_ν and q_ν, and the centrifugal distortion constants, D_ν, which are several times as large as the values of these parameters. For this reason, these parameters are not shown in Table IV. The Λ-doubling parameters could be determined more precisely if more Q-branch transitions were measured; this would require higher resolution measurements since the Q-branch transitions are so closely spaced.

TABLE IV. Best-fit parameters for C_4^-. All parameters are in cm^{-1}. Uncertainties in parentheses are 1σ error bars.

	Parameters	Present work	*Ab initio* theory[a]
$X\ ^2\Pi_g$ state	B_0	0.166 63(22)	0.166 10(40)
	A_0	−39(9)	
$C\ ^2\Pi_u$ state	T_0	21 871.525(7)	22 599
	B_0	0.156 51(25)	0.155 20(40)
	A_0	−37(9)	
Between states	$B_0''(X)-B_0'(C)$	0.010 12(13)	0.010 90(60)
	$A_0''-A_0'$	−1.536(7)	
	$D_0''-D_0'$	$1.1(3)\times10^{-9}$	
	T_1	22 623.96(11)	
$C\ ^2\Pi_u$ state:	B_1	0.156 34(26)	
(2_0^1 level)	A_1	−33(9)	
	α_1	$17(16)\times10^{-5}$	
	$A_0''-A_1'$	−6.45(10)	

[a]From Ref. 18.

Since no transitions between F_1 and F_2 manifolds were observed, A_v'' and A_v' are highly correlated, and this is the origin of their large error bars. However, for the origin band, the difference $\Delta A = (A_0'' - A_0')$ is accurately determined and found to be approximately equal to the experimental $R_{1/2}-R_{3/2}$ band head spacing of 1.7 cm^{-1}. For the 2_0^1 band, no transitions in the $\Omega=1/2$ manifold were assigned, so the spin–orbit constant A_1' in Table IV is obtained from the $R_{1/2}-R_{3/2}$ band head spacing of 6.45 cm^{-1} and the best-fit A_0'' value of the X state. As shown in Table IV, this yields effective spin–orbit constants for the $v_2=0$ and $v_2=1$ levels of the $C\ ^2\Pi_u$ state that differ by $\sim$5 cm^{-1}.

Such an effect can occur in a polyatomic $^2\Pi$ state through Fermi resonance interactions with nearby vibrational levels with the same vibronic symmetry. For example, in the $C\ ^2\Pi_u$ state, the $v_5=2$ level, with two quanta in a degenerate bending mode, lies about 300 cm^{-1} below the $v_2=1$ level (see Fig. 1). The $v_5=2$ level is split into several components resulting from a combination of Renner–Teller and spin–orbit interactions.[30] The differing strengths of interactions between the $^2\Pi_{1/2}$ and $^2\Pi_{3/2}$ components of the $v_2=1$ level with components of the same symmetry in the $v_5=2$ level may be sufficient to change the splitting in the $v_2=1$ level relative to the ground state by the observed amount, 5 cm^{-1}.

Similar but larger effects have been seen in the $X\ ^2\Pi$ and $B\ ^2\Pi$ states of the NCO radical.[31] For example, in the 1_0^1 band of the $B\leftarrow X$ electronic transition, the $^2\Pi_{1/2}-^2\Pi_{1/2}$ and $^2\Pi_{3/2}-^2\Pi_{3/2}$ sub-bands are split by 64 cm^{-1}, rather than 19 cm^{-1} as would be expected from the difference $A''-A'$ determined from the origin band. This is attributed to the two spin–orbit components of the (100) vibrational state of NCO $B\ ^2\Pi$ electronic state experiencing different strengths of Fermi interaction with the nearby (020) bending levels. In the NCO $B\ ^2\Pi$ state, the (100) and (020) levels are calculated to lie only 40 cm^{-1} apart,[32] considerably less than the analogous spacing in the C_4^- $C\ ^2\Pi_u$ state ($\sim$300 cm^{-1}). On the other hand, the magnitude of the perturbation in C_4^- is also smaller. The key to determining whether this mechanism is operative in C_4^- would be to obtain a high resolution scan of the 5_0^2 band, but we were unable to obtain a rotationally resolved spectrum of this feature at our laser resolution. Thus, while the exact nature of the perturbation in the C_4^- $C\ ^2\Pi_u$ state is unknown, this type of Fermi resonance interaction is certainly a reasonable candidate.

Given the spectroscopic constants, the spectrum has been simulated by assuming a Boltzmann distribution for the anion population. The simulated spectrum of the origin band, along with the experimental spectrum, is shown in Fig. 4. Relative line intensities in each manifold are calculated from

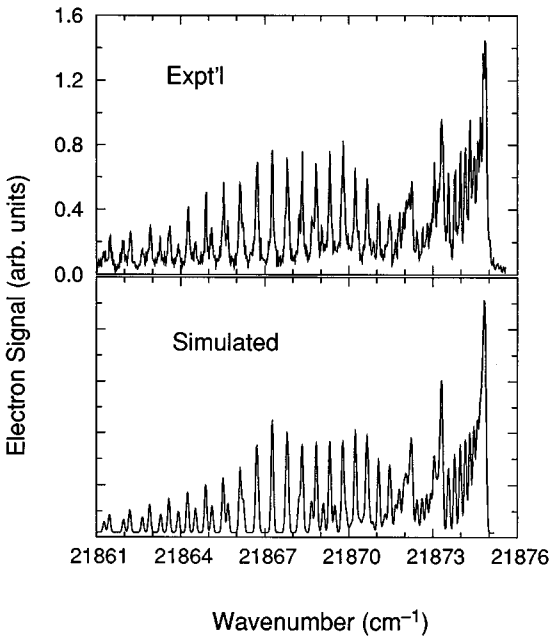

FIG. 4. Comparison of experimental with simulated rotational spectrum of the origin band using fitted molecular constants.

the product of the line strength, determined by Hönl–London formulas[33] for a $^2\Pi \leftarrow ^2\Pi$ transition and the Boltzmann factor. A rotational temperature of 35 K and spin–orbit temperature of 45 K were used in calculating Boltzmann factors. Peak widths in the simulation at FWHM are assumed to be 0.10 cm^{-1}, resulting mostly from the laser linewidth combined with some residual power broadening. Overall, the agreement between the simulated and experimental spectra is very good.

We close by considering a possible connection between the results presented here and earlier experiments by Zajfman *et al.*[34] In those experiments, hot C_4^- anions produced in a sputtering source were found to have a much lower detachment threshold, ~2.1 eV, than C_4^- produced in laser vaporization/pulsed beam sources (3.88 eV).[11,12] These results were used to infer the existence of a cyclic form of C_4^- with a lower electron binding energy than linear C_4^-. However, our results show that cold, linear C_4^- readily undergoes resonant two-photon detachment starting at 2.7 eV. Thus, the C_4^- produced in the sputtering source may have been undergoing two-photon rather than one-photon detachment; the lower threshold could easily be due to hot band transitions due to the high internal temperature of anions produced by sputtering. Zajfman *et al.* did find a linear dependence of electron yield on laser power, but our experiments indicate that the bound–bound excitation transition saturates very easily, so that a linear power dependence does not rule out a two-photon process. Hence, it is quite possible that Zajfman *et al.* were observing two-photon detachment from vibrationally excited linear anions, rather than one-photon detachment from cyclic anions. These issues and a more complete discussion of multiphoton detachment dynamics in carbon cluster anions will be discussed more fully in an upcoming publication.[23]

V. CONCLUSIONS

Resonant two-photon detachment spectroscopy provides a sensitive means of studying electronic transitions in mass-selected negative ions. In this paper, R2PD has been used to study the $C\ ^2\Pi_u \leftarrow X\ ^2\Pi_g$ electronic transition in C_4^-. The one-color detachment spectrum of C_4^- reveals vibrational structure of the excited anion state, and confirms that the band seen previously by Maier in the same spectral region is from C_4^-. The two-color detachment spectrum, taken under conditions which reduce power broadening, shows rotationally resolved bands of the $C\ ^2\Pi_u \leftarrow X\ ^2\Pi_g$ electronic transition. The observed rotational structure confirms the assignment of these two electronic states of C_4^-. The molecular constants obtained for these two states are in good agreement with the results of high level *ab initio* calculations.

This technique can be applied to study other negative ions with allowed electronic transitions below the electron affinity, including C_5^-, C_6^-, and other even-numbered carbon cluster anions.[14,35] The characterization of the excited electronic states of these anions will be invaluable in future experiments in which stimulated Raman pumping coupled with resonant two-photon detachment will be used to determine vibrational frequencies of the anion ground states. We have recently published the results of such an experiment on C_2^-,[36] and the existence of excited states for the larger carbon cluster anions suggests that these species, too, can be investigated with stimulated Raman pumping.

ACKNOWLEDGMENT

This work is supported by the Air Force Office of Scientific Research under Grant No. F49620-94-1-0115.

[1] K. S. Pitzer and E. Clementi, J. Am. Chem. Soc. **81**, 4477 (1959).
[2] W. Weltner, Jr. and R. J. van Zee, Chem. Rev. **89**, 1713 (1989).
[3] J. R. Heath and R. J. Saykally, in *On Clusters and Clustering, From Atoms to Fractals*, edited by P. J. Reynolds (Elsevier, Amsterdam, 1993), pp. 7–21.
[4] T. F. Giesen, A. van Orden, H. J. Hwang, R. S. Fellers, R. A. Provencal, and R. J. Saykally, Science **265**, 756 (1994).
[5] G. Herzberg and A. Lagerqvist, Can. J. Phys. **46**, 2363 (1968).
[6] P. L. Jones, R. D. Mead, B. E. Kohler, S. D. Rosner, and W. C. Lineberger, J. Chem. Phys. **73**, 4419 (1980).
[7] U. Hefter, R. D. Mead, P. A. Schulz, and W. C. Linberger, Phys. Rev. A **28**, 1429 (1983).
[8] R. D. Mead, U. Hefter, P. A. Schulz, and W. C. Lineberger, J. Chem. Phys. **82**, 1723 (1985).
[9] B. D. Rehfuss, D.-J. Liu, B. M. Dinelli, M.-F. Jagod, W. C. Ho, M. W. Crofton, and T. Oka, J. Chem. Phys. **89**, 129 (1988).
[10] H. S. Carman and R. N. Compton, J. Chem. Phys. **98**, 2473 (1993), and references therein.
[11] S. Yang, K. J. Taylor, M. J. Craycraft, J. Conceicao, C. L. Pettiette, O. Cheshnovsky, and R. E. Smalley, Chem. Phys. Lett. **144**, 431 (1988).
[12] D. W. Arnold, S. E. Bradforth, T. N. Kitsopoulos, and D. M. Neumark, J. Chem. Phys. **95**, 8753 (1991).
[13] G. V. Helden, P. R. Kemper, N. G. Gotts, and M. T. Bowers, Science **259**, 1300 (1993).
[14] P. Freivogel, J. Fulara, M. Jakobi, D. Forney, and J. P. Maier, J. Chem. Phys. **103**, 54 (1995).
[15] J. D. Watts, I. Cernusak, and R. J. Bartlett, Chem. Phys. Lett. **178**, 259 (1991); J. D. Watts and R. J. Bartlett, J. Chem. Phys. **101**, 409 (1994).
[16] L. Adamowicz, J. Chem. Phys. **94**, 1241 (1991).
[17] L. Adamowicz, Chem. Phys. **156**, 387 (1991).
[18] S. Schmatz and P. Botschwina, Int. J. Mass Spec. Ion Proc. **149**, 621 (1995).
[19] W. C. Lineberger and T. A. Patterson, Chem. Phys. Lett. **13**, 40 (1972).
[20] C. C. Arnold, Y. Zhao, T. N. Kitsopoulos, and D. M. Neumark, J. Chem. Phys. **97**, 6121 (1992).
[21] T. N. Kitsopoulos, I. M. Waller, J. G. Loeser, and D. M. Neumark, Chem. Phys. Lett. **159**, 300 (1989).
[22] D. L. Osborn, D. J. Leahy, D. R. Cyr, and D. M. Neumark, J. Chem. Phys. **104**, 5026 (1996).
[23] Y. Zhao, E. de Beer, C. Xu, T. R. Taylor, and D. M. Neumark, J. Chem. Phys. (in press).
[24] T. N. Kitsopoulos, C. J. Chick, Y. Zhao, and D. M. Neumark, J. Chem. Phys. **95**, 5479 (1991).
[25] I. Kopp and J. T. Hougen, Can. J. Phys. **45**, 581 (1967).
[26] J. M. Brown, J. T. Hougen, K.-P. Huber, J. W. C. Johns, I. Kopp, H. Lefebvre-Brion, A. J. Merer, D. A. Ramsay, J. Rostas, and R. N. Zare, J. Mol. Spectrosc. **55**, 500 (1975).
[27] R. N. Zare, A. L. Schmeltekopf, W. J. Harrop, and D. L. Albritton, J. Mol. Spectrosc. **46**, 37 (1973).
[28] D. M. Neumark, K. R. Lykke, T. Andersen, and W. C. Lineberger, J. Chem. Phys. **83**, 4364 (1985).
[29] W. H. Press, S. A. Teukolsky, W. T. Vetterling, and B. P. Flannery, *Numerical Recipes in Fortran* (Cambridge U.P., Cambridge 1992), 2nd ed., pp. 678–683.
[30] G. Herzberg, *Electronic Structure of Polyatomic Molecules* (Van Nostrand, New York, 1966), p. 35.
[31] R. N. Dixon, Can. J. Phys. **38**, 10 (1960); D. R. Cyr, R. E. Continetti, R. B. Metz, D. L. Osborn, and D. M. Neumark, J. Chem. Phys. **97**, 4937 (1992); M. Wu and T. J. Sears, Mol. Phys. **82**, 503 (1994).
[32] M. H. Alexander and H.-J. Werner (private communication).

[33] G. Herzberg, *Molecular Spectra and Molecular Structure, Vol. I* (Van Nostrand, Princeton, NJ, 1950), p. 208.
[34] D. Zajfman, H. Feldman, O. Heber, D. Kella, D. Majer, Z. Vager, and R. Naaman, Science **258**, 1129 (1992).
[35] M. Ohara, H. Shiromaru, Y. Achiba, K. Aoki, H. Hashimoto, and S. Ikuta, J. Chem. Phys. **103**, 10393 (1995).
[36] E. de Beer, Y. Zhao, I. Yourshaw, and D. M. Neumark, Chem. Phys. Lett. **244**, 400 (1995).